Characteristics of Observed Atmospheric Circulation Patterns Associated with Temperature Extremes over North America

PAUL C. LOIKITH AND ANTHONY J. BROCCOLI

Department of Environmental Sciences, Rutgers, The State University of New Jersey, New Brunswick, New Jersey

(Manuscript received 2 December 2011, in final form 4 April 2012)

ABSTRACT

Motivated by a desire to understand the physical mechanisms involved in future anthropogenic changes in extreme temperature events, the key atmospheric circulation patterns associated with extreme daily temperatures over North America in the current climate are identified. The findings show that warm extremes at most locations are associated with positive 500-hPa geopotential height and sea level pressure anomalies just downstream with negative anomalies farther upstream. The orientation, physical characteristics, and spatial scale of these circulation patterns vary based on latitude, season, and proximity to important geographic features (i.e., mountains, coastlines). The anomaly patterns associated with extreme cold events tend to be similar to, but opposite in sign of, those associated with extreme warm events, especially within the westerlies, and tend to scale with temperature in the same locations. Circulation patterns aloft are more coherent across the continent than those at the surface where local surface features influence the occurrence of and patterns associated with extreme temperature days. Temperature extremes may be more sensitive to small shifts in circulation at locations where temperature is strongly influenced by mountains or large water bodies, or at the margins of important large-scale circulation patterns making such locations more susceptible to nonlinear responses to future climate change. The identification of these patterns and processes will allow for a thorough evaluation of the ability of climate models to realistically simulate extreme temperatures and their future trends.

1. Introduction

Temperature extremes are expected to change in severity, frequency, and duration as a result of anthropogenic global warming with an increase in warm events and a decrease in cold events likely, resulting from a shift in the temperature frequency distribution toward higher values (Easterling et al. 2000; Meehl and Tebaldi 2004; Tebaldi et al. 2006; Meehl et al. 2007). Extreme heat events such as those seen in western Europe in 2003 and Russia in 2010, while very unusual in the current climate, are expected to become more commonplace in a warmer world (e.g., Beniston 2004; Schär et al. 2004; Stott et al. 2004; Dole et al. 2011; Rahmstorf and Coumou 2011). Such changes would leave the population of the world vulnerable to extremes that it is not prepared to deal with and in many locations has never experienced before (Meehl et al. 2009). To better anticipate these changes, more work is needed to understand the physical mechanisms involved with extreme temperature events in the current climate.

Indices of extreme events have been devised and evaluated and consistently show a warming of nighttime temperatures and fewer extreme cold events on global and regional scales (Frich et al. 2002; Alexander et al. 2006; Griffiths and Bradley 2007; Brown et al. 2010). Recent studies using observations and model simulations suggest that the detected warming trend in warm nights (Morak et al. 2011) and extreme warm daytime temperatures (Christidis et al. 2011) is at least partially attributable to anthropogenic external forcing. Tebaldi et al. (2006), using general circulation model (GCM) simulations of extreme temperature indices from a suite of models, show that models project a continuation of the already observed trends in the increasing occurrence of warm extremes and decreases in cold extremes. Extreme value statistics have been used to show global and regional changes in observed temperature extremes (Brown et al. 2008) and evidence suggests an

Corresponding author address: Paul C. Loikith, Rutgers University, Department of Environmental Sciences, 14 College Farm Road, New Brunswick, NJ 08901.
E-mail: ploikith@envsci.rutgers.edu

DOI: 10.1175/JCLI-D-11-00709.1

anthropogenic signal in these changes (Zwiers et al. 2011). Extreme value statistics have also been applied to GCM simulations and show an overall warming in extremes with the warming on the cold tail being of the greatest magnitude (Kharin and Zwiers 2000, 2005; Kharin et al. 2007).

Hegerl et al. (2004) suggest that detection of changes in mean temperature cannot be substituted for changes in extremes for most parts of the world. As a result of changes in circulation, there is evidence of regions where extreme cold events may not become less common and in some cases will occur with greater frequency (Vavrus et al. 2006; Kodra et al. 2011). Strong circulation anomalies at 500 hPa have been linked to extreme warm temperature events (Meehl and Tebaldi 2004), and the strength of many recurrent circulation patterns of both local and hemispheric extent have been shown to be important in extreme temperature days. Cassano et al. (2011) showed the strong associations with preferred circulation patterns and anomalous temperatures over Alaska. Teleconnections related to unusual deviations in the index values of larger scale recurrent modes of low frequency variability have also been associated with extreme temperature events, especially in the Northern Hemisphere winter months (Thompson and Wallace 2001; Wettstein and Mearns 2002; Quadrelli and Wallace 2004; Kenyon and Hegerl 2008).

This project aims to gain a better understanding of the mechanisms responsible for temperature extremes in the recent climate over North America. Motivated by the growing body of evidence suggesting that anthropogenic changes in temperature extremes are occurring on global and regional scales already, we identify the large-scale circulation patterns associated with extreme temperature days for the entire continent of North America and describe how these patterns depend on geographic location, season, and type of extreme (warm or cold). In the remainder of the paper we describe our data and analysis methodology in section 2. In section 3 we present the results of our analysis and describe the key atmospheric circulation patterns associated with temperature extremes. In section 4 we take a closer look at specific cases to identify how these patterns vary with location. The final section summarizes our findings and conclusions along with implications for future work.

2. Data and methodology

a. Data

Daily temperature extremes were obtained from the HadGHCND gridded daily temperature dataset. The dataset is a joint project between the Met Office Hadley Centre for Climate Prediction and Research and the U.S. National Climatic Data Center (NCDC). The dataset is on a global domain and the majority of the observations that are applied to the gridding process are from the NCDC Global Historical Climatology Network-Daily (GHCND). The resolution of the grid is 2.5° latitude by 3.75° longitude. The dataset has two products: gridded observed daily maximum and minimum temperatures from 1946 to 2000 and gridded daily maximum and minimum temperature anomalies from 1950 to 2007. We primarily make use of the anomalies in this work, which are computed by subtracting the 5-day running mean of a 30-yr daily climatology (1961–90) from the actual temperature. A more detailed description of the dataset and the gridding process can be found in Caesar et al. (2006).

Circulation patterns were calculated using data from the National Centers for Environmental Prediction Reanalysis 1 (Kalnay et al. 1996). To calculate anomalies in reanalysis variables we utilized the same method and reference period as Caesar et al. for the gridded temperature anomalies. The resolution of the reanalysis data is higher than the HadGHCND at 2.5° by 2.5°.

b. Methodology

Extreme temperatures were defined as those days when the daily maximum or minimum temperature anomaly was above the 95th or below the 5th percentile in the temperature anomaly frequency distribution for a particular calendar month during the period 1961–90. This 30-yr period was chosen as a compromise between the conflicting goals of maximizing the sample size of extreme events while minimizing the effect of temperature trends in recent decades. The months of January, April, July, and October were analyzed to represent the four standard seasons. Anomalies were used rather than temperature to avoid temporal biases associated with systematic variations in climatological mean temperature during the course of a calendar month; such biases would be acute during the transition seasons. Although warming has occurred during the period of analysis, the extreme events are relatively well distributed in time and, thus, the warming did not impact or bias our results in a meaningful way.

The foundation of our results is the analysis of composites of atmospheric circulation variables, with emphasis on anomalies in 500-hPa geopotential height Z_{500}, and sea level pressure (SLP). Anomalies were calculated by subtracting the 5-day running mean from a 30-yr climatology from the actual SLP or Z_{500} value for each day. To create the composites, the global anomalies for each of the warmest or coldest days at

a particular grid cell were extracted from the reanalysis and then averaged. The sample size is 47 days for 31-day months and 45 for 30-day months [5% of 31 (30) days × 30 years]; however, if there was a tie for the 45th or 47th most extreme day, all days with the same value were included. It is inherent in our method that events consisting of several consecutive days of extreme temperatures were included, thus not all patterns in the composites are fully independent.

To allow for systematic comparison of circulation patterns from different locations, composite patterns were regridded from absolute geographic coordinates to a polar coordinate grid (radial resolution of 250 km and azimuthal resolution of 2°) that is defined in relation to the grid cell at which the temperature extremes occurred. An example of one such "gridcell-relative grid" is shown in Fig. 1. The outer boundary of the grid is located 4500 km from the central grid cell, a distance chosen empirically such that the large-scale and local circulation patterns would be included.

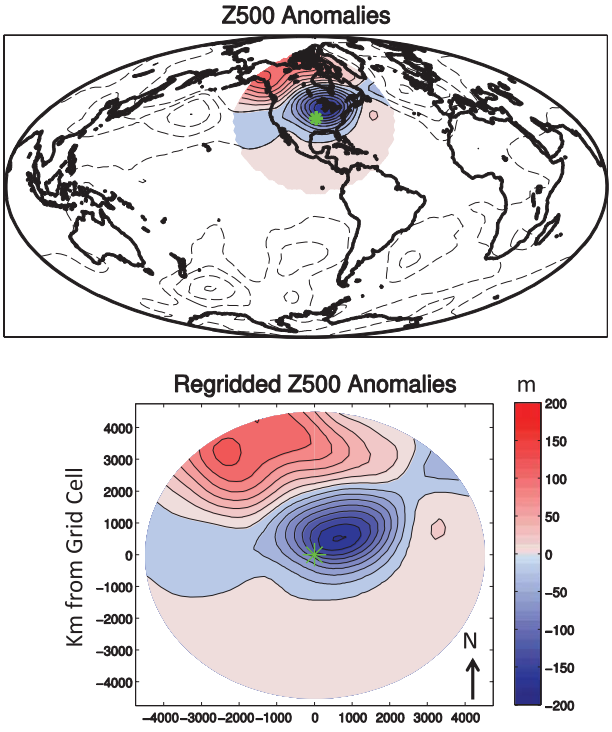

FIG. 1. An illustration of how the gridcell-relative composites were created: (top) map of Z_{500} anomalies associated with January extreme cold days at the grid cell represented by the green star. Only data within 4500 km of the grid cell is shaded. (bottom) The above map is interpolated onto the gridcell-relative grid such that the center of the circle is the grid cell where the extreme temperatures are being computed. This was done for all grid cells over North America for all composites.

3. Composite analysis

Gridcell-relative composites were developed for all combinations of extremes, seasons, and circulation variables, but the bulk of the analysis in this section is focused on extremes occurring in January and July. In the discussion that follows, daily maxima and minima at or below the 5th percentile are denoted by Tx5 and Tn5, respectively, while those at or above the 95th percentile are denoted by Tx95 and Tn95. While January Tx5 and Tn5 (cold winter days/nights) and July Tx95 and Tn95 (warm summer days/nights) are associated with the majority of climate impacts, we also include warm winter extremes (January Tx95 and Tn95) and cold summer extremes (July Tx5 and July Tn5) to present a comprehensive analysis of the mechanisms associated with days in the tails of the temperature distribution.

a. Description of domainwide patterns

For each type of temperature extreme (i.e., Tx5, Tn5, etc.), composite circulation patterns were computed for each of the 315 grid cells in North America, defined here as all land area north of 17.5°N bounded by the Atlantic and Pacific Oceans on the east and west respectively. The resulting gridcell-relative maps are too numerous to be presented or readily interpreted, thus their content has been summarized by averaging the composite circulation patterns for each type of extreme over the entire analysis domain to produce a "grand composite." Grand composites for each type of extreme are depicted by Fig. 2, with SLP anomalies indicated by shading and Z_{500} anomalies by contours. The median value of the pattern correlations between the grand composite and all of the individual composites is provided as a metric of the ability of the grand composite to capture the common features of the individual composites. January extremes are characterized by strong Z_{500} anomalies (~150 m) located near or slightly to the east of the location experiencing the temperature extreme. The pattern associated with extreme cold maximum temperatures is very similar to that for extreme cold minimum temperatures; however, the negative height anomaly center is shifted slightly east in the Tn5 case for January when compared with the Tx5 case. The upstream positive SLP anomaly center also extends closer to the central point in the January Tn5 case. While this shift is subtle and may be due to sampling, it can be understood from a synoptic perspective as conditions ideal for radiational cooling (calm winds, clear skies) often lead to the coldest nighttime temperatures. In the Tn5 case, the largest positive SLP anomalies are nearly overhead, favoring such conditions, and at Z_{500} the axis of the trough is slightly downstream, signifying the end of cold advection. Extreme cold maximum temperatures do not have this eastward shift as ongoing advection of the coldest air is

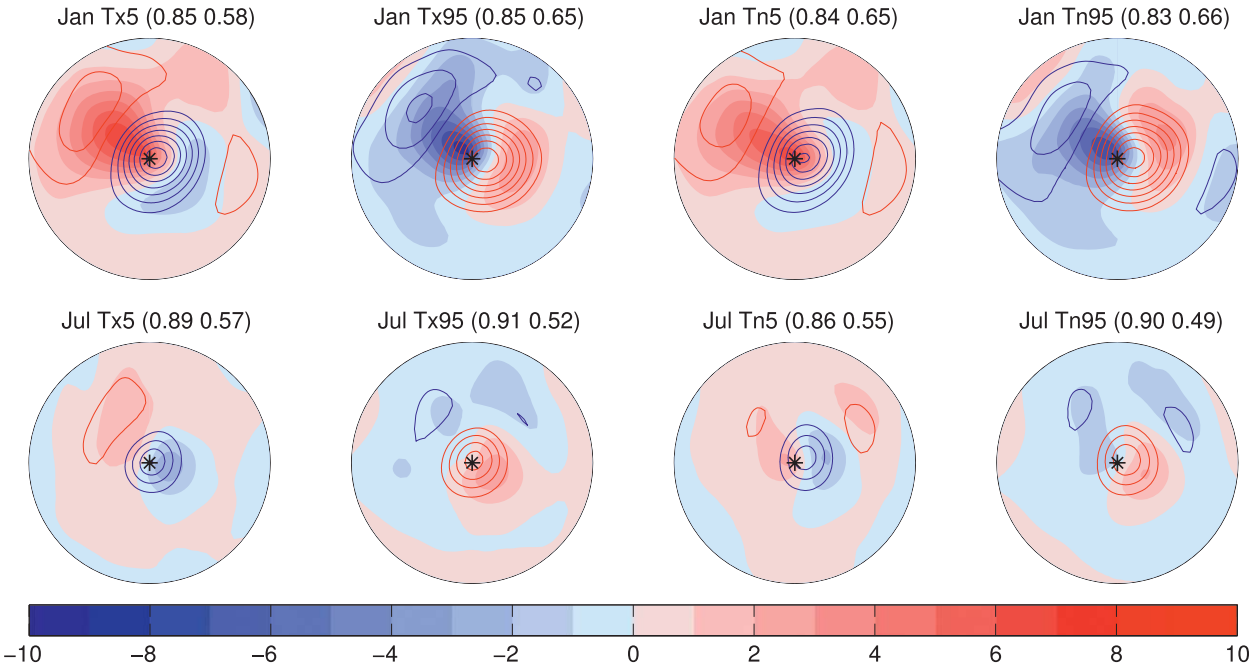

FIG. 2. Grand composites of anomalies for all 315 grid cells: SLP anomalies (hPa) are shaded and Z_{500} height anomalies are contoured every 20 m; red (blue) contours are positive (negative) Z_{500} anomalies. Grand composites are shown for (top) January and (bottom) July extreme (from left to right) cold maximum (Tx5), warm maximum (Tx95), cold minimum (Tn5), and warm minimum (Tn95) temperatures. Values to the right of the labels represent the median pattern correlation coefficient when the grand composite for (left) Z_{500} and (right) SLP is correlated with all individual composites for the entire continent.

still needed to suppress maximum temperatures. Extreme warm January maximum temperatures are characterized by a very strong positive Z_{500} anomaly and a strong negative SLP anomaly to the west of the grid cell. At the surface this results in a strong southerly component to the flow, which favors warm advection at most locations.

July extremes are associated with weaker anomalies than in January. Northern Hemisphere summer is characterized by a retreat of the westerlies to the north and a weakening of the zonal temperature gradient. This results in less potential for strong, large-scale circulations to develop along temperature gradients that can lead to the advection of anomalous temperatures. The Z_{500} pattern still has a center of positive (for warm) and negative (for cold) anomalies nearby or downstream; however, these anomalies are of smaller magnitude and spatial scale than those seen in January. The shape of the anomalies is also more rounded than in January, likely a result of the fact that unusual perturbations in the Z_{500} field in the summer are often cutoff from the mean flow—unlike the highly amplified ridges and troughs seen in the winter. Additionally, when averaged across the continent, the pattern is more equivalent barotropic in the summer than in winter when a noticeable upstream oriented vertical tilt is seen between the surface and the Z_{500} level. In general, the composite patterns are consistent with simple dynamical balance considerations.

Empirical orthogonal function (EOF) analysis was performed on the composite patterns for all 315 grid cells for each type of extreme. In this application, EOF analysis is used to identify spatial covariability across grid cells rather than spatial covariability across time. With the EOF analysis performed in this manner, the variance explained by the first EOF is greatly separated from subsequent EOFs. The patterns for the leading EOF (Fig. 3) largely resemble the grand composites in Fig. 2, especially where the variance explained by the first EOF is high. The lower percentage of variance explained in the SLP patterns is indicative of greater spatial variability or a lack of a consistent pattern throughout the domain when compared to the patterns at Z_{500}. The lack of a preferred pattern, especially at the surface, suggests that differing local patterns are being averaged away in computing the grand composite. Pattern correlation coefficients between the first EOF and the grand composite of the corresponding variable and type of extreme are very close to one for Z_{500} and range from 0.6 to 0.9 for SLP for both months. The relative magnitudes of the explained variance resemble the relative magnitudes of median correlation coefficient values in Fig. 2.

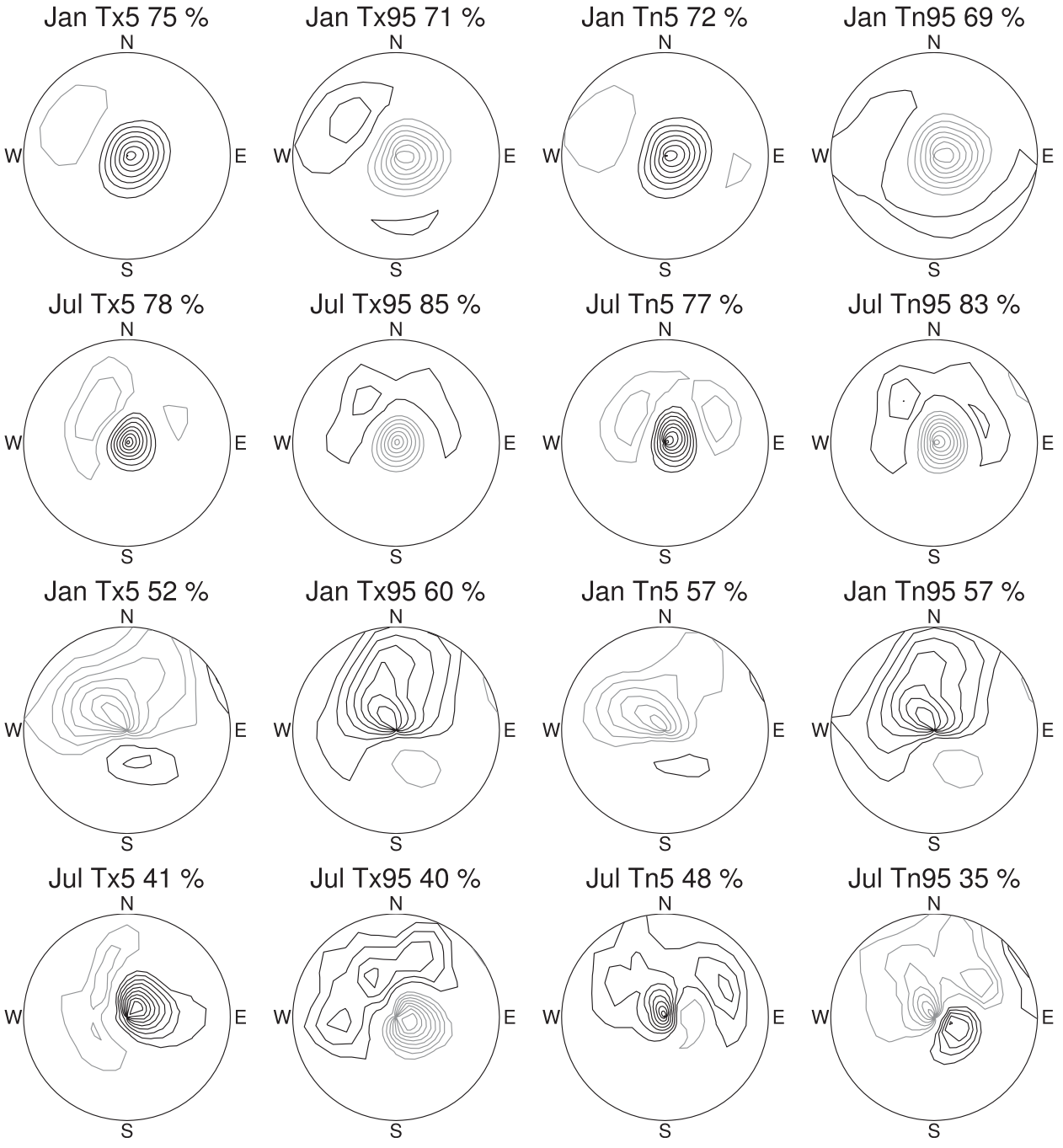

FIG. 3. The leading EOF of (top two rows) Z_{500} and (bottom two rows) SLP obtained when EOF analysis is performed on the 315 different composites for each grid cell in North America. Black contours are positive values and gray contours are negative. The variance explained by each first EOF is plotted with the title. The types of extremes match those of Fig. 2.

To see where the composite patterns at individual grid cells most resemble the grand composite, pattern correlations between the anomaly pattern at each grid cell and the grand composite are plotted in Fig. 4. In general, the pattern correlations at Z_{500} are high, indicating that the local patterns resemble the grand composites. Some exceptions are in the extreme southern extent of the domain, south of the main storm track, with this area expanding northward in July. The atmosphere within this region lacks strong thermal contrasts, resulting in weak and variable circulation patterns associated with extreme temperature days when compared

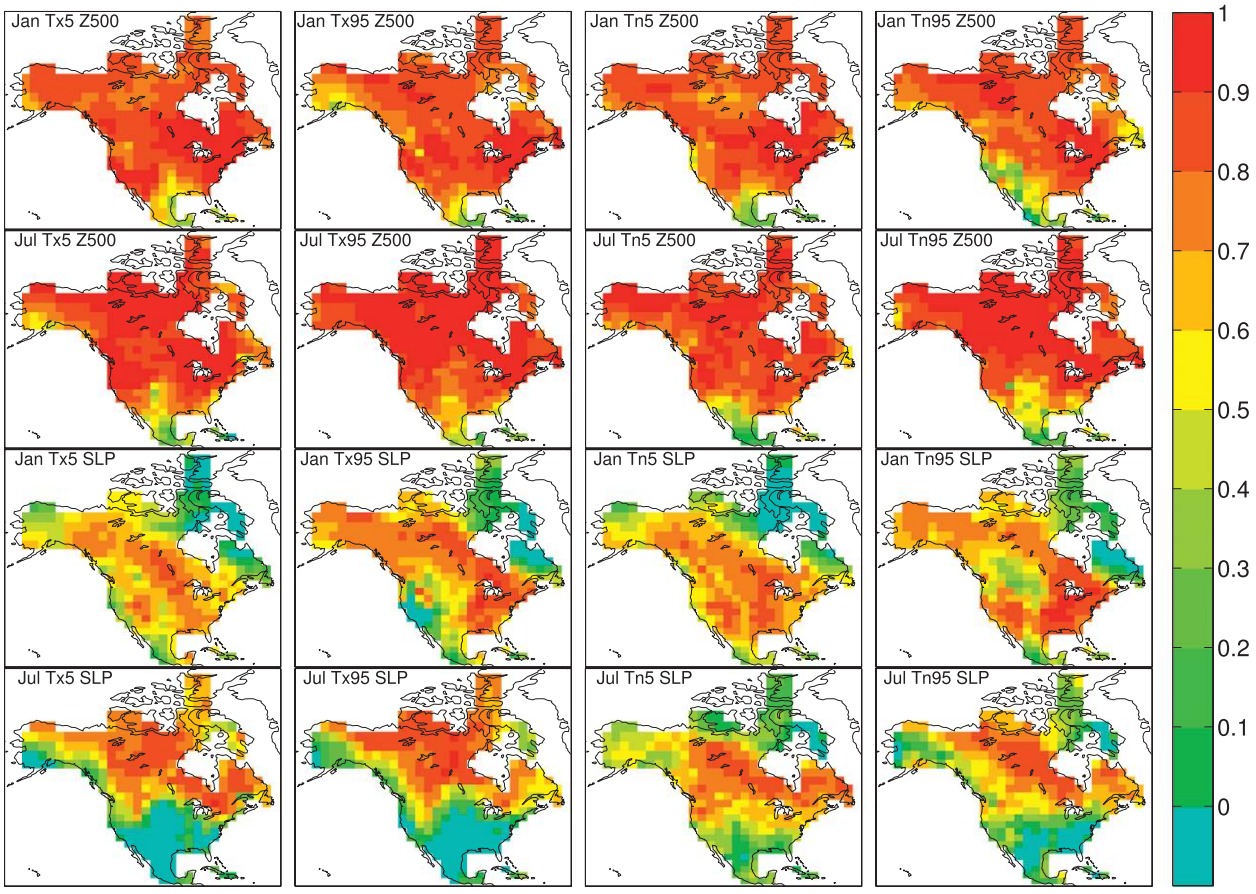

FIG. 4. Coefficients from a pattern correlation between the composite pattern at each grid cell and the corresponding grand composite in Fig. 2. Higher values (red pixels) indicate places where the local pattern resembles the grand composite for the indicated extreme. Areas where the correlation is less than 0 are shaded in blue.

with areas farther north. The pattern correlations in January in the Rocky Mountains and along the U.S. West Coast are lower for extreme warm minimum temperatures than extreme warm maximum temperatures, indicative of regional differences there. At the surface, SLP anomaly patterns in general do not resemble the grand composites as strongly as at Z_{500}. The lower resemblance suggests more variety in the possible SLP patterns associated with extreme temperature days than at Z_{500}. The resemblance is particularly poor in far northeastern North America in January and south of the main belt of the westerlies in July where atmospheric baroclinicity is low. In less baroclinic environments, extreme temperatures are less associated with robust large-scale circulation anomalies and more with local processes and surface moisture anomalies as was seen during the 2003 European heat wave (Fischer et al. 2007; Weisheimer et al. 2011).

Skewness of the temperature frequency distribution helps identify regions where local circulation patterns are associated with days in the tails of the distribution. Furthermore, the degree of temperature skewness may indicate how sensitive a location will be to changes in extreme temperatures as a result of anthropogenic global warming (Ruff and Neelin 2012). For example, far northeastern North America is both dominated by positive skew (Fig. 5) and weak or negative correlation with the grand composites. Here a long warm tail is associated with incursions of air from the relatively warm ocean to the east while extremely cold temperatures are associated with a westerly trajectory. This contrasts with locations in the main belt of the westerlies in which the coldest air arrives from the north and the warmest air from the south, leading to a band of low skewness in interior portions of the continent. Farther south, skewness is predominantly negative where infrequent outbreaks of cold air invade a relatively mild region.

b. *Variability within composite patterns*

Places where the local composites do not resemble the grand composites raise the question: are the patterns in

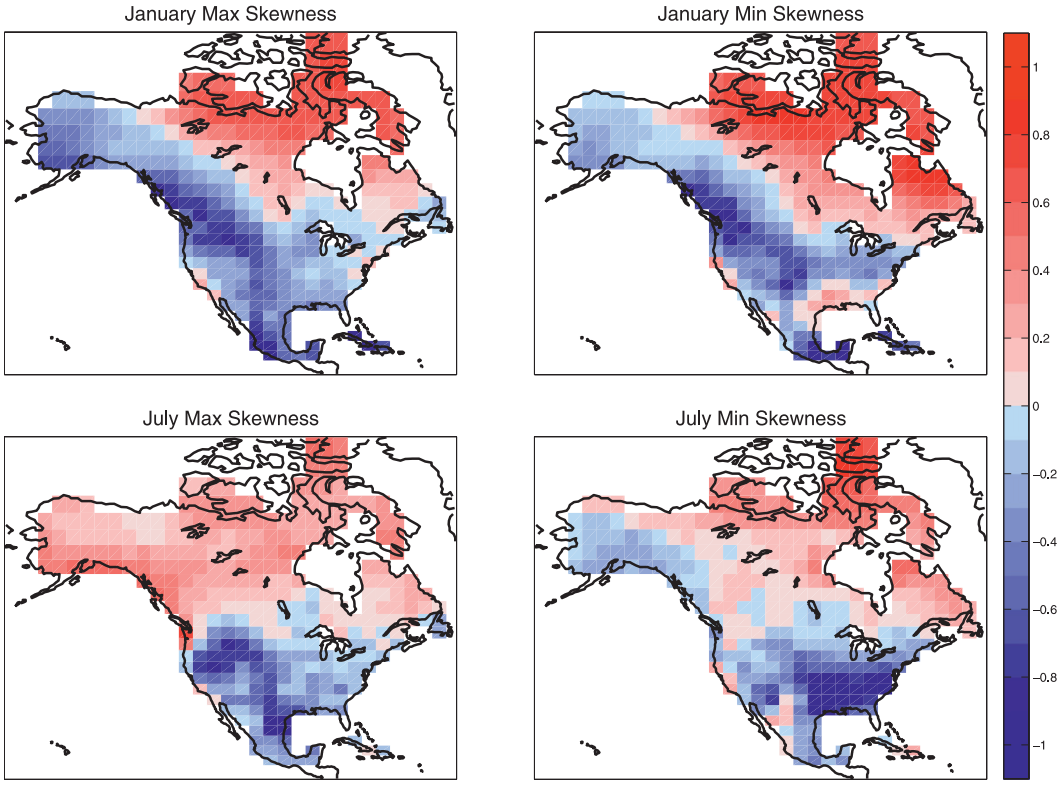

FIG. 5. Plots of skewness for (top) January and (bottom) July maximum and minimum temperature anomalies for all 30 years of data.

these areas resulting from distinctly different processes than the areas that do resemble the grand composites or do these areas lack a preferred circulation pattern associated with temperature extremes? To answer this question, an EOF analysis was performed on the daily anomaly patterns that make up each local composite. The variance explained by the leading EOF of the composite patterns is plotted in Fig. 6. Locations in which the leading EOF accounts for a higher percentage of variance have more of a preferred pattern associated with temperature extreme days, while lower values of explained variance imply more variability among the circulation anomaly patterns associated with extreme temperature days.

In general, the results from this local EOF analysis do not support the hypothesis that locations in which local composites are poorly correlated with the grand composites lack a preferred circulation pattern associated with temperature extremes. For instance, variance explained by the first EOF is relatively high in northeastern North America despite the weak correlations between the local composites and grand composites evident in Fig. 4. Thus the lack of similarity between the local composites and the grand composites in that region is likely due to regional differences in the preferred circulation pattern associated with temperature extremes.

More generally, the percentage of variance explained by the leading EOF is higher in January than July and higher for Z_{500} than SLP. There is a discernible tendency for larger explained variance for warm extremes than cold extremes in January, particularly for SLP, which may be because warm extremes in winter are more advectively than radiatively driven. An area of relatively high explained variance exists in the central part of the continent associated with extreme cold days in July at the surface, while the same region has relatively low variance explained by the first EOF for Z_{500}. This may be due to cloudiness and precipitation inhibiting the daytime temperature rise during upslope flow events, which are typically confined to the lower troposphere.

c. *Pattern symmetry and linearity*

Pattern symmetry describes how similar, but opposite in sign, the anomaly patterns associated with cold extremes are to those associated with warm extremes. A metric of pattern symmetry (Fig. 7) is developed by computing the pattern correlation between the composite pattern associated with extreme cold days and extreme warm days and reversing its sign. Thus a grid cell for which the composite patterns for warm extremes

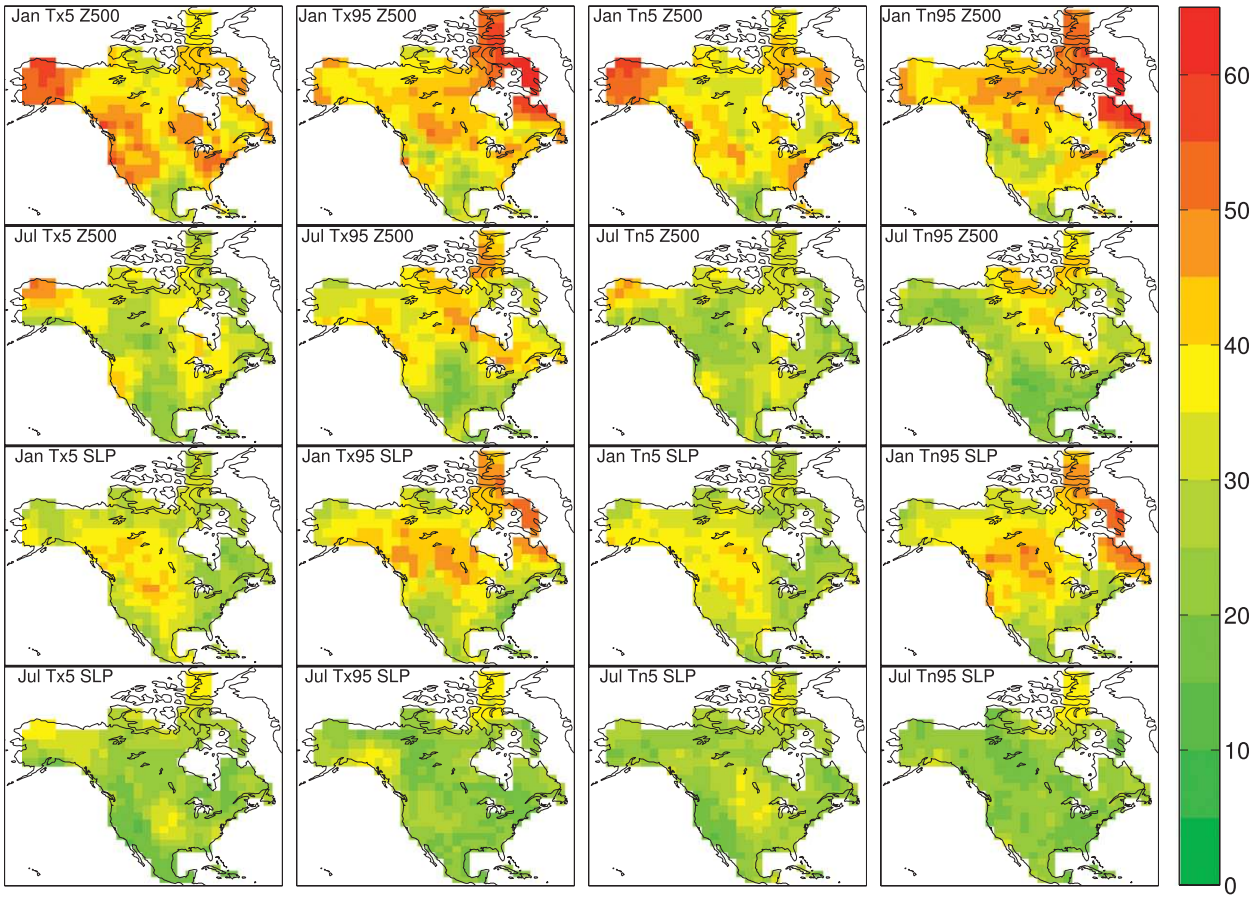

FIG. 6. Variance explained (%) by the leading EOF of the daily patterns comprising the composite for each grid cell for the indicated extreme. Areas with higher variance explained have less variability within the composites.

is exactly opposite to the pattern for cold extremes would have a symmetry value of one.

An additional property of interest is the linearity of the composite patterns. A circulation pattern can be regarded as linear if the pattern for the largest daily temperature anomalies is a higher amplitude version of the pattern associated with smaller temperature anomalies, with the amplitude proportional to the magnitude of the temperature anomaly. A second metric is developed to assess pattern linearity according to the following procedure: for each grid cell over North America, circulation anomalies at all locations in the domain are regressed on the temperature anomaly at that grid cell for all days in the sample. This yields a pattern of regression coefficients that have units of height per degree (for Z_{500}) or pressure per degree (for SLP). To allow for more interpretable comparisons between these patterns and the composite anomaly patterns determined from the tails of the temperature anomaly distribution, each regression coefficient is multiplied by the mean temperature anomaly for the days making up the composite, producing a pattern of regression-derived circulation anomalies with the same units as the composites. The rms difference between each composite anomaly pattern and the regression-derived anomaly pattern, normalized by the standard deviation of the composite anomaly pattern, is then defined as a metric of pattern linearity (Fig. 8). The pattern linearity would be zero in a case in which the composite anomaly pattern scales linearly in the temperature anomaly. A value of one would indicate that the rms difference between the composite anomaly pattern and the regression-derived anomaly pattern is as large as the spatial variability of the pattern itself, which would be indicative of considerable nonlinearity. Note that symmetry is expressed by one value that compares both warm and cold composites, whereas linearity is expressed by two values, one each for warm and cold composites.

Circulation patterns are generally more symmetrical and linear at Z_{500} than at sea level. Both symmetry and linearity are the smallest across the continent in the July

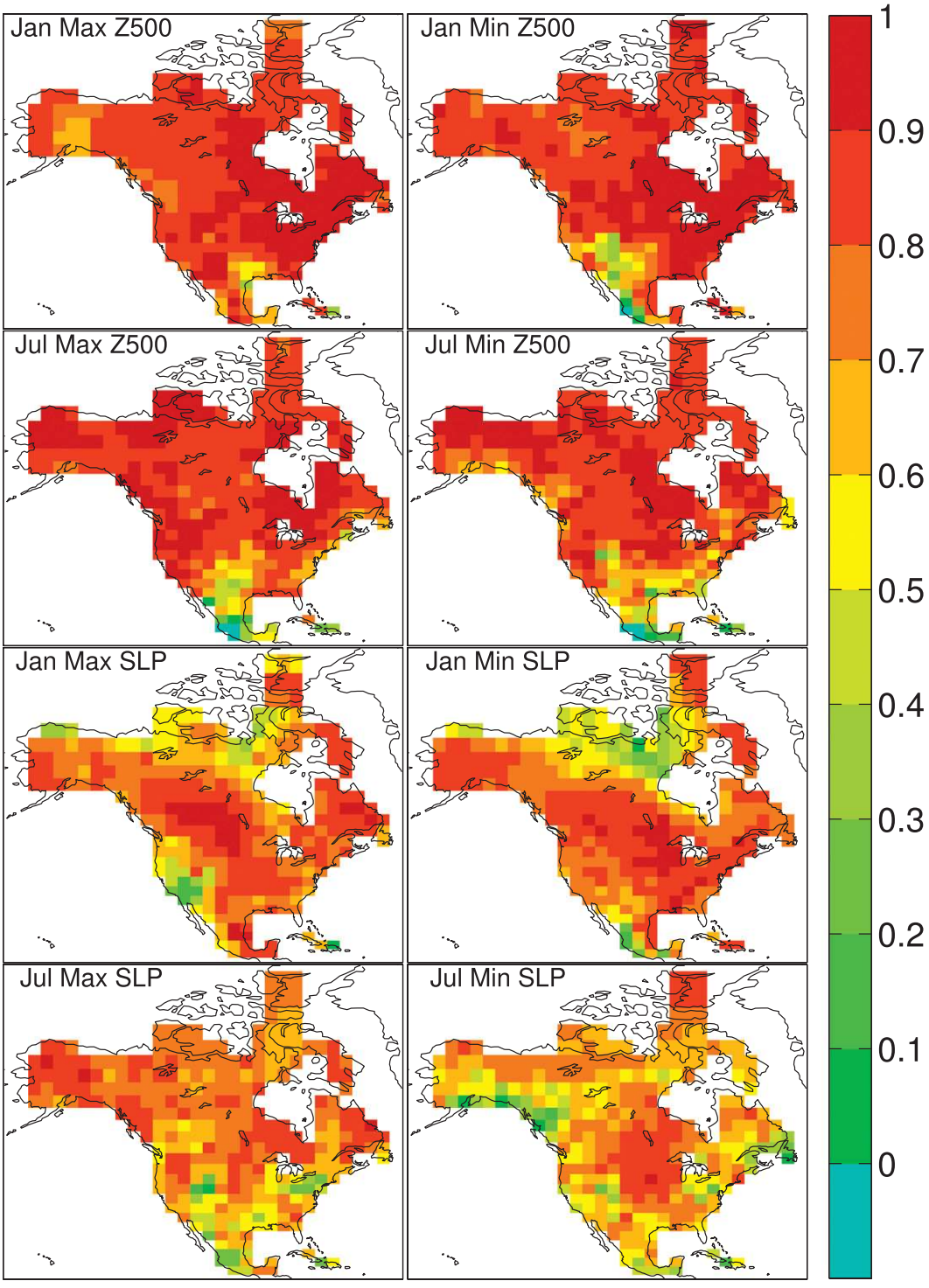

FIG. 7. Maps of symmetry computed by calculating the coefficients from a pattern correlation between the composite pattern for extreme warm days and extreme cold days. Each coefficient was multiplied by −1 so that a higher positive correlation equates to areas with more symmetrical pattern pairs. The (top) Z_{500} and (bottom) SLP anomaly patterns are shown. Plots labeled "Min" are the correlation between the extreme cold minimum and the extreme warm minimum; the plots labeled "Max" are for the extremes in maximum temperatures.

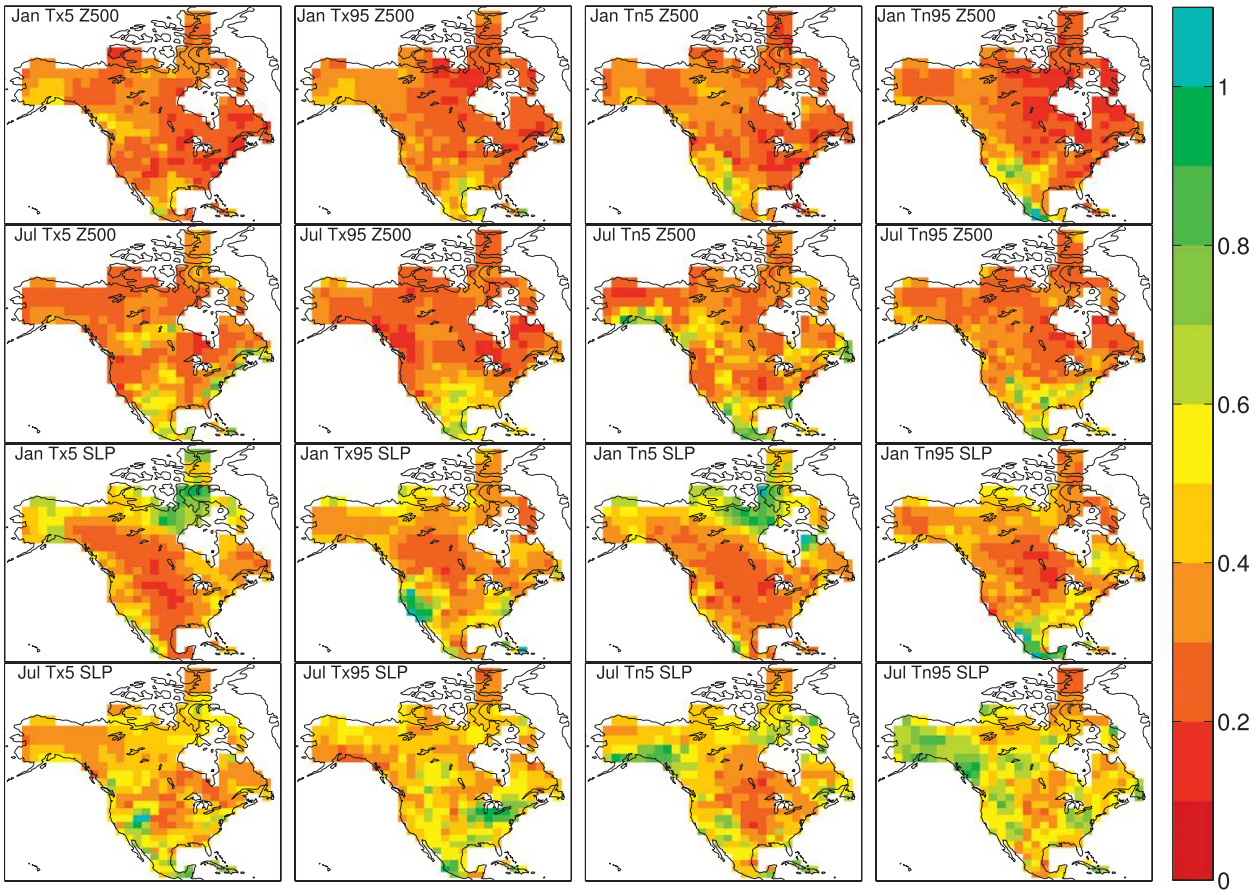

FIG. 8. Maps of linearity, calculated by computing the rms error between the composite pattern for each grid cell and the linear regression pattern for each grid cell. The regression pattern is computed by regressing the entire time series of (top rows) Z_{500} anomalies and (bottom rows) SLP for each grid cell on the entire time series of temperature anomalies at the grid cell where the extreme temperatures are occurring. The regression coefficients are multiplied by the mean temperature anomaly in the specific tail so that both composite patterns and regression patterns have the same units. The rms error is normalized by the standard deviation of the composite pattern. Higher values indicate where the patterns are less linear and lower values where patterns are more linear.

SLP cases, which may result from those patterns being less dependent on large-scale circulation patterns and more dependent on local processes and land surface coupling. Patterns in SLP anomalies associated with cold January days have weaker symmetry and linearity in a band stretching from north-central Canada southeastward across Hudson Bay. This indicates that the circulation patterns associated with days in the cold tail of the temperature distribution are different than those associated both with the warm tail and nonextreme temperature days. This area also correlates to a region of positively skewed temperature distributions (Fig. 5). SLP patterns have weak symmetry and low linearity values in the U.S. Southwest associated with Tx95 events in January and in the vicinity of the Great Lakes during July extreme warm days. In general, the most symmetrical and linear patterns are found in the main belt of the westerlies, shifting meridionally with the seasons.

d. Spatial scale of patterns

The distance between the center of the greatest positive and negative anomalies in Z_{500} composite patterns (normalized by the standard deviation of the Z_{500} anomalies in this case), or the "half-wavelength" of the wave pattern, was calculated for each grid cell. The median distance value was calculated for all grid cells in three latitude bands and plotted in Fig. 9. With a few exceptions in the lowest latitude band, January has the longest half-wavelength and July has the shortest. The spatial scale of the transition seasons tends toward intermediate values that are larger than July but smaller than January. With a few exceptions, the northernmost band has the longest half-wavelengths and the southernmost has the shortest. There is very little difference between the half-wavelengths of the higher two latitude bands in all cases except for Tx95 where the difference is relatively large. The lowest latitude

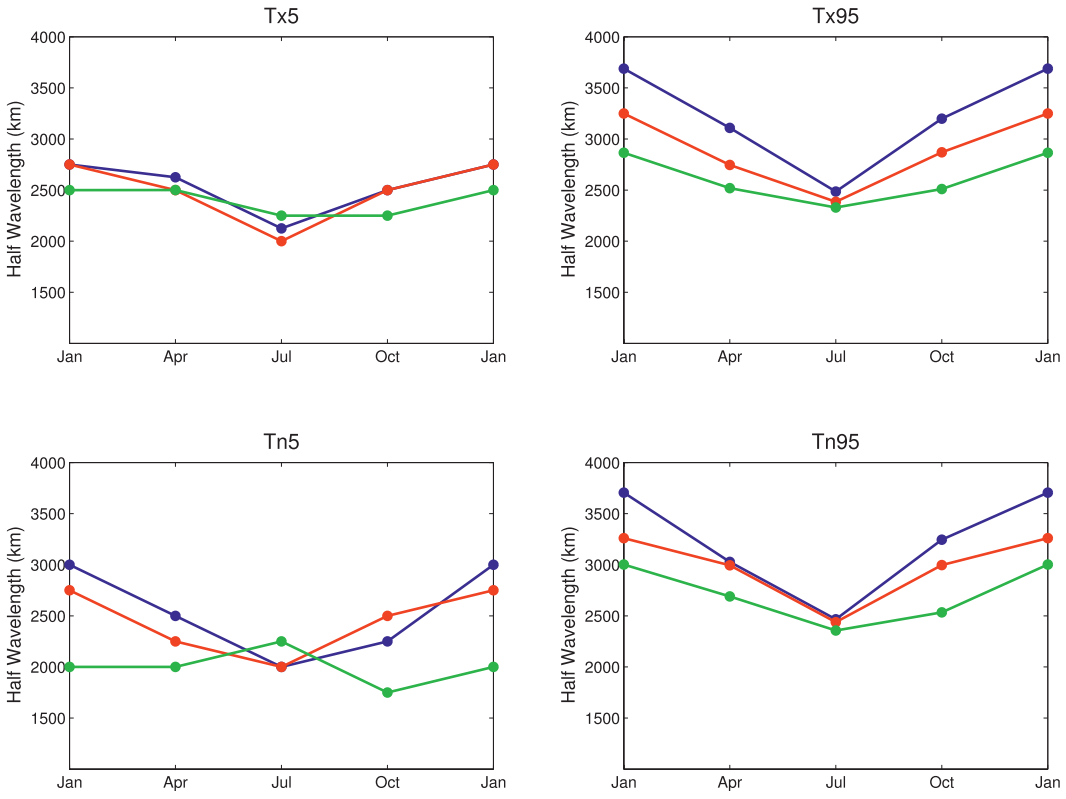

FIG. 9. The median half-wavelengths for three latitude bands for the entire seasonal cycle as represented by the four months analyzed. Each half-wavelength is the distance in kilometers (y axis) between the largest positive and negative normalized anomalies in Z_{500}. The median is computed from the half-wavelength values for every grid cell north of 57.5°N (blue), between 37.5° and 57.5°N (red), and south of 37.5°N (green).

band (south of 37.5°N) has little or no discernible seasonal cycle in all cases but Tn95. This lack of seasonal cycle may be due to the lesser influence of midlatitude synoptic-scale systems at lower latitudes. In all cases the half-wavelengths are within the synoptic-scale and in some instances smaller in scale than larger-scale recurrent teleconnection patterns, suggesting that a substantial influence on extreme temperature days comes from transient weather patterns.

4. Select cases

The following section examines composite patterns associated with temperature extremes for four different grid cells, each chosen to provide examples of different circulation characteristics as described in the previous section. Each composite is calculated for a specific grid cell; however, the composite patterns can be assumed to be representative of nearby locations.

a. Interior North America: January Z_{500} Tn5 and Tn95

Figure 10 shows maps of the Z_{500} composite pattern for extreme warm (left) and extreme cold (right) minimum temperature days in January in the far interior of the continent. This is an area characterized by patterns that are relatively linear and symmetrical and a have a strong resemblance to the grand composite for Z_{500}. The extreme warm events are associated with a strong positive anomaly near the location where the extreme temperature is occurring with a ring of negative anomalies surrounding the positive anomaly center. The composite pattern for extremely cold events is similar but opposite in sign. This region is situated such that air trajectories from the colder north and warmer south are unimpeded by terrain and not influenced by large bodies of water. The result is strong symmetry in circulation patterns associated with days in the tails and patterns that scale with temperature. The composite pattern is larger in spatial scale than the grand composite, yet the local circulation anomalies at Z_{500} are similar to those seen in the grand composite. The large-scale ridge and trough pattern at Z_{500} is indicative of a highly amplified wintertime synoptic pattern with little discernible influence from local or regional geography.

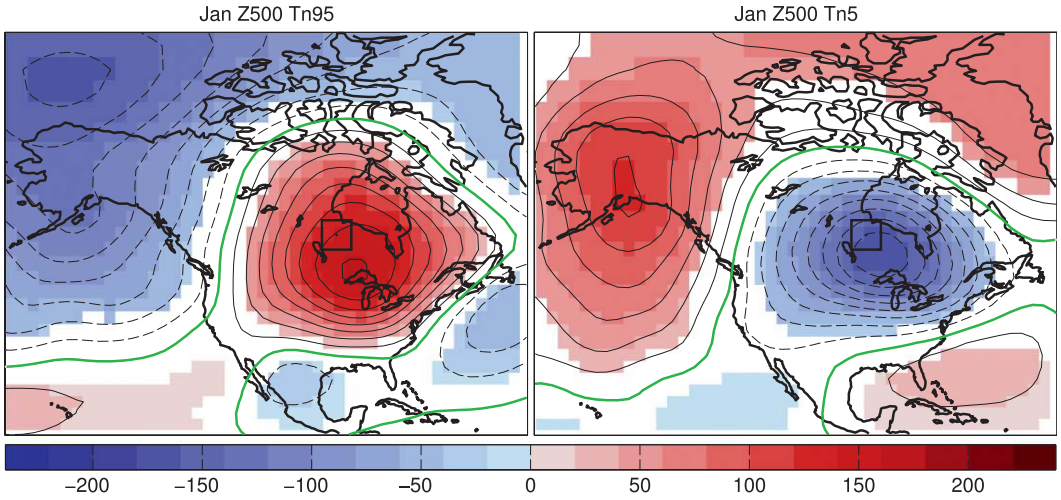

FIG. 10. Composite patterns of the anomalies in Z_{500} (contoured every 20 m) in the area highlighted by the black box concurrent with (left) extreme warm and (right) extreme cold daily minimum temperatures in January. The thick green line is the 0-m contour. Only values statistically significant at the 5% level are shaded.

b. Central United States: July Tx95 Z_{500} and SLP

Meehl and Tebaldi (2004) show that anomalous circulation at Z_{500} was associated with the high impact events of the Chicago heat wave in 1995 and the European heat wave in 2003. Figure 11 shows the composite for Z_{500} and SLP anomalies associated with the warmest 5% of days in the south-central part of the continent. The anomalies in July are weaker than in January; however, the anomalies in Z_{500} and SLP are largely statistically significant at the 5% level (shaded areas in Fig. 11). At Z_{500} a positive anomaly is nearly overhead or slightly to the north of the region, which is similar to the pattern associated with the 1995 heat wave that affected this region. This implies that the 1995 anomaly pattern is representative of days in the top 5% of the distribution. At the surface, anomalies in SLP are weakly negative across the region.

The variance explained by the first EOF of the patterns contributing to the composites is relatively low at Z_{500} and correlation with the grand composites is relatively low at Z_{500} and negative for SLP. The weak anomalies at the surface may indicate that there are other processes, such as low soil moisture content,

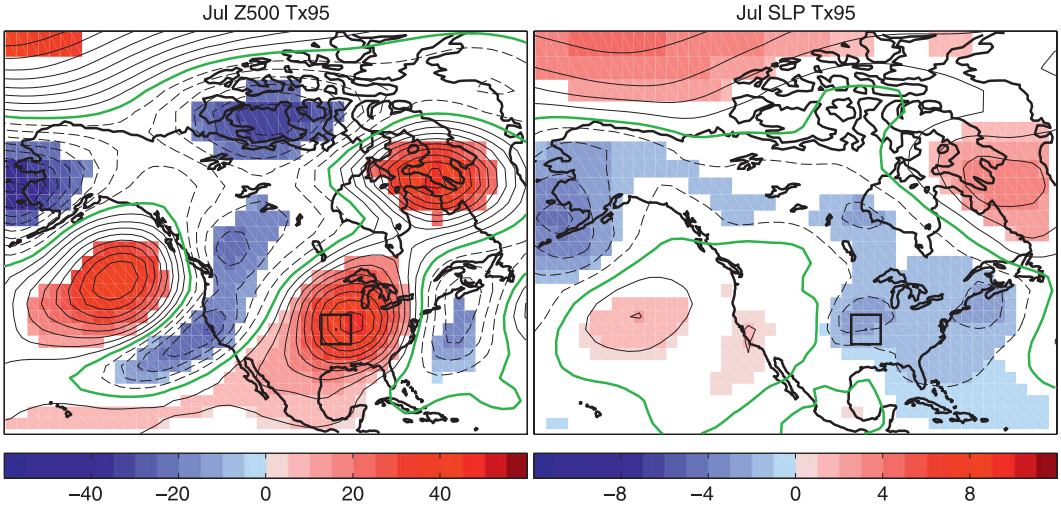

FIG. 11. Composite patterns of the anomalies in (left) Z_{500} (contours every 5 m) and (right) SLP (contours every 1 hPa) in the area highlighted by the black box for extreme warm daily maximum temperatures in July. The thick green line is the 0-m hPa^{-1} contour. Only values statistically significant at the 5% level are shaded.

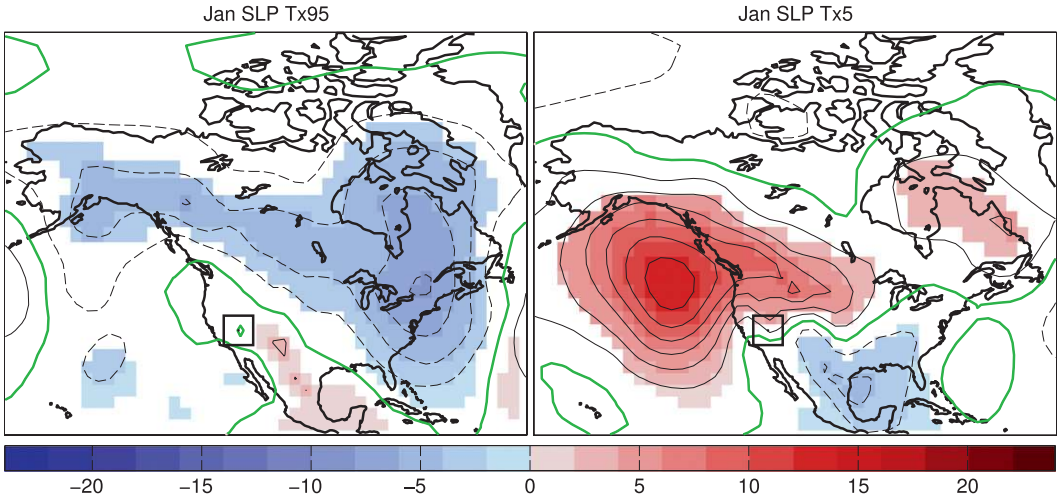

FIG. 12. Composite patterns of the anomalies in SLP (contoured every 2 hPa) in the area highlighted by the black square concurrent with (left) extreme warm and (right) extreme cold daily maximum temperatures in January. The thick green line is the 0-hPa contour. Only values statistically significant at the 5% level are shaded.

associated with extreme warm temperature days in this region. The Z_{500} anomalies are indicative of a wave train, with other strong anomalies upstream and downstream of the primary positive anomaly center. Lau and Nath (2012) have found a similar wave train pattern in their analysis of North American heat waves.

c. *Southwest United States: January SLP Tx5 and Tx95*

Figure 12 shows SLP anomaly composites associated with extreme warm (left) and cold (right) temperature days in the southwest part of the continent. This is a region characterized by very weak linearity in the Tx95 case and very weak symmetry in the SLP composites associated with extreme warm temperature days. The SLP anomaly pattern that is associated with extreme cold days is characterized by a strong high pressure anomaly to the north and west and a weaker negative anomaly to the south and east. This sets up a strong pressure gradient that allows for surface advection from the north. A slight change in surface wind direction would result in less cold air as advection with a westerly component would have influence from the Pacific Ocean and advection from the interior of the continent would result in advection of desert air rather than air originating in the Arctic.

Extremely warm days in this location are not associated with a localized large scale anomaly pattern in SLP. This suggests that local, smaller-scale processes are likely responsible for extreme warm days in this region, possibly related to topographical features that cannot be resolved at this scale. The greater symmetry and linearity of the patterns associated with extreme warm minimum temperatures suggests that advection on the large-scale is more important for nighttime extreme temperatures.

d. *Eastern Alaska: January and April SLP Tx5 and Tx95*

In most cases, composites of daily anomaly patterns associated with temperature extremes in the transition seasons (spring and fall) share commonalities with those in the winter and summer; however, in this case, unique processes contribute to very different regimes in transition seasons. Figure 13 shows composites of SLP associated with extreme maximum temperature days in eastern Alaska and far northwestern Canada. January extreme warm and cold maximum temperatures are associated with relatively high values of symmetry in SLP composites. Following the SLP anomaly contours, anomalous advection of air from the south at the surface is associated with extreme warm days and anomalous advection with an easterly trajectory is associated with extreme cold days. Insolation is negligible in January in this region, leaving surface advection as the primary factor in the occurrence of extreme temperatures. In April the composite pattern associated with extreme cold days is similar to January, but the pattern associated with extreme warm days is very different. A broad area of positive SLP anomalies is situated over the region with little or no surface wind anomalies. Advection from the south would have marine influence from the relatively cold Pacific and would inhibit the development of a warm air mass. As a result, conditions associated with extreme warm maximum temperature days favor ample sunshine and light winds under high surface pressure.

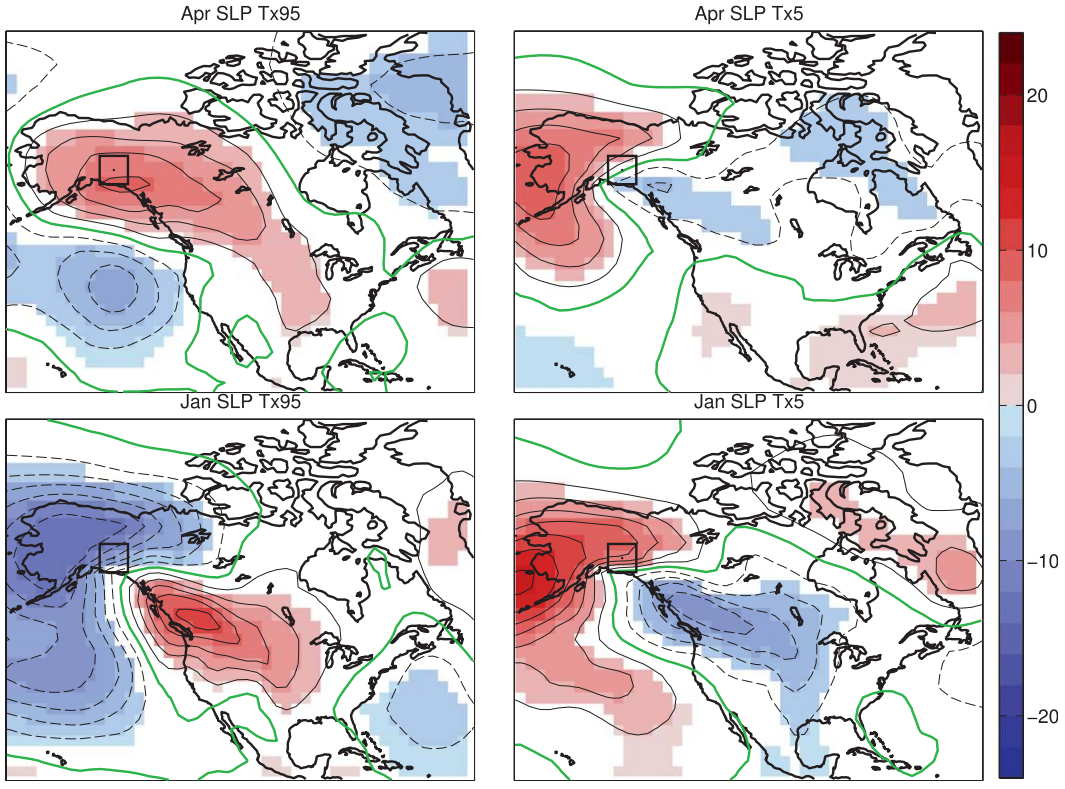

FIG. 13. Composite patterns of the anomalies in SLP (contoured every 2 hPa) in the area highlighted by the black box concurrent with (left) extreme warm and (right) extreme cold daily maximum temperatures in (top) April and (bottom) January. The thick green lines are the 0-hPa contour. Only values statistically significant at the 5% level are shaded.

Composite analysis of total flow (not shown) shows extreme warm temperatures in January associated with a strengthened and expanded Aleutian low coupled with a strong high pressure center over western North America resulting in a strong pressure SLP gradient. In April, extreme warm maximum temperatures are associated with a southwestward shift of the Aleutian low and a high pressure center to the east of the region, resulting in weak surface winds and advection. Extreme cold temperatures for both months are associated with a low SLP center to the southeast of the region and high pressure to the north resulting in advection from the relatively cold east and northeast at the surface. The complex interaction between temperature and the trajectory of surface advection and how this changes with season suggests that this is a region in which temperature extremes may be sensitive to relatively modest shifts in circulation. As an example, a circulation anomaly that increases the amount of onshore synoptic-scale flow in this region would likely lessen the number of extreme warm days. While the winter months may not be as sensitive to subtle changes in circulation, April would experience nonlinear changes in temperature extremes under such a hypothetical change in circulation.

5. Summary and concluding remarks

Key atmospheric circulation patterns associated with extreme temperature days have been systematically investigated for all of North America. Warm extremes are associated with positive anomalies in the Z_{500} and SLP field downstream of a location experiencing extreme temperatures with negative anomalies upstream in most cases. Composites of anomalies in Z_{500} and SLP generally have stronger magnitudes and larger spatial scales in January than in July with the transition seasons reflecting characteristics of both seasons. Patterns associated with extreme warm and cold days are the most symmetrical and linear at Z_{500} and in January. Local topographical influences as well as the influence from local land surface characteristics and proximity to large bodies of water affect the symmetry and linearity of the composite patterns. Locations in the westerlies tend to resemble the grand composites better than areas outside of this region, and SLP composites are more spatially variable than Z_{500}. In some cases, regions that do not resemble the grand composite patterns have a preferred, but different, composite pattern as indicated by relatively low variability between the daily patterns contributing

to the composite. The variance explained by the first EOF of all composite patterns for a given extreme is higher for Z_{500} than SLP.

The results of this work suggest that some places may be more sensitive to subtle shifts in circulation that could occur as a result of anthropogenic climate change. Expected changes in storm tracks (Yin 2005) and expansion of the area influenced by tropical circulation (Lu et al. 2007; Seidel et al. 2008) are both examples of changes in circulation that could yield nonlinear impacts on local temperature. Regions where temperature is strongly influenced by large bodies of water or land surface conditions (such as the eastern Alaska/northwestern Canada example in section 4d) could also experience nonlinear impacts from shifts in circulation or changes in ocean temperature or land surface characteristics. Regions within the westerlies, where the circulation anomalies associated with extreme temperature days are currently made up of unusually strong weather disturbances, could end up in a less baroclinic environment as the earth warms, resulting in weaker circulation anomalies.

The spatial scales of the Z_{500} and SLP anomaly patterns generally fall within the synoptic scale. While some patterns visually suggest influence from large-scale teleconnection patterns (not shown), such as the Arctic Oscillation and the Pacific–North American pattern, there is a major influence from local synoptic-scale weather perturbations in each composite pattern, especially within the westerlies. The spatial scales of the circulation patterns tend to be smaller in July as the atmospheric is less baroclinic, and extremes are likely influenced by smaller-scale and physical processes not represented in the composites. A more thorough analysis of the relationship of temperature extremes to modes of climate variability will be the subject of subsequent research. Additional information about surface moisture anomalies and local smaller-scale circulation would help shed light on the mechanisms associated with extremes in the warmer months and south of the westerlies. Future work will also evaluate how well climate models simulate the circulation patterns associated with daily temperature extremes and the extent to which such patterns change in global warming simulations.

Acknowledgments. This study was supported by the Office of Science (BER), U.S. Department of Energy, Award DE-SC0005467. We thank Gabriel Lau, Ben Lintner, and John Lanzante for useful discussions and insight throughout the project. We also thank Ben Lintner and the anonymous reviewers for their helpful and constructive comments on earlier versions of this paper.

REFERENCES

Alexander, L. V., and Coauthors, 2006: Global observed changes in daily climate extremes of temperature and precipitation. *J. Geophys. Res.,* **111,** D05109, doi:10.1029/2005JD006290.

Beniston, M., 2004: The 2003 heat wave in Europe: A shape of things to come? An analysis based on Swiss climatological data and model simulations. *Geophys. Res. Lett.,* **31,** L02202, doi:10.1029/2003GL018857.

Brown, P. J., R. S. Bradley, and F. T. Keimig, 2010: Changes in extreme climate indices for the Northeastern United States, 1870–2005. *J. Climate,* **23,** 6555–6572.

Brown, S. J., J. Caesar, and C. A. T. Ferro, 2008: Global changes in extreme daily temperature since 1950. *J. Geophys. Res.,* **113,** D05115, doi:10.1029/2006JD008091.

Caesar, J., L. Alexander, and R. Vose, 2006: Large-scale changes in observed daily maximum and minimum temperatures: Creation and analysis of a new gridded data set. *J. Geophys. Res.,* **111,** D05101, doi:10.1029/2005JD006280.

Cassano, E. N., J. J. Cassano, and M. Nolan, 2011: Synoptic weather pattern controls on temperature in Alaska. *J. Geophys. Res.,* **116,** D11108, doi:10.1029/2010JD015341.

Christidis, N., P. A. Stott, and S. Brown, 2011: The role of human activity in the recent warming of extremely warm daytime temperatures. *J. Climate,* **24,** 1922–1930.

Dole, R., and Coauthors, 2011: Was there a basis for anticipating the 2010 Russian heat wave? An analysis based on Swiss climatological data and model simulations. *Geophys. Res. Lett.,* **38,** L06702, doi:10.1029/2010GL046582.

Easterling, D. R., G. A. Meehl, C. Parmesan, S. A. Changnon, T. R. Karl, and L. O. Mearns, 2000: Climate extremes: Observations, modeling, and impacts. *Science,* **289,** 2068–2074.

Fischer, E. M., S. I. Seneviratne, P. L. Vidale, D. Lüthi, and C. Schär, 2007: Soil moisture–atmosphere interactions during the 2003 European summer heat wave. *J. Climate,* **20,** 5081–5099.

Frich, P., V. Alexander, P. Della-Marta, B. Gleason, M. Haylock, A. M. G. Klein Tank, and T. Peterson, 2002: Observed coherent changes in climatic extremes during the second half of the twentieth century. *Climate Res.,* **19,** 193–212.

Griffiths, M. L., and R. S. Bradley, 2007: Variations of twentieth-century temperature and precipitation extreme indicators in the Northeast United States. *J. Climate,* **20,** 5401–5417.

Hegerl, G. C., F. W. Zwiers, P. A. Stott, and V. V. Kharin, 2004: Detectability of anthropogenic changes in annual temperature and precipitation extremes. *J. Climate,* **17,** 3683–3700.

Kalnay, E., and Coauthors, 1996: The NCEP/NCAR 40-Year Reanalysis Project. *Bull. Amer. Meteor. Soc.,* **77,** 437–471.

Kenyon, J., and G. C. Hegerl, 2008: Influence of modes of climate variability on global temperature extremes. *J. Climate,* **21,** 3872–3889.

Kharin, V. V., and F. W. Zwiers, 2000: Changes in the extremes in an ensemble of transient climate simulations with a coupled atmosphere–ocean GCM. *J. Climate,* **13,** 3760–3788.

——, and ——, 2005: Estimating extremes in transient climate change simulations. *J. Climate,* **18,** 1156–1173.

——, ——, X. Zhange, and G. C. Hegerl, 2007: Changes in temperature and precipitation extremes in the IPCC ensemble of global coupled model simuations. *J. Climate,* **20,** 1419–1444.

Kodra, E., K. Steinhaeuser, and A. R. Ganguly, 2011: Persisting cold extremes under 21st-century warming scenarios. *Geophys. Res. Lett.,* **38,** L08705, doi:10.1029/2011GL047103.

Lau, N.-C., and M. J. Nath, 2012: A model study of heat waves over North America: Meteorological aspects and projections for the 21st century. *J. Climate,* **25,** 4761–4784.

Lu, J., G. A. Vecchi, and T. Reichler, 2007: Expansion of the Hadley cell under global warming. *Geophys. Res. Lett.,* **34,** L06805, doi:10.1029/2006GL028443.

Meehl, G. A., and C. Tebaldi, 2004: More intense, more frequent, and longer lasting heat waves in the 21st century. *Science,* **305,** 994–997.

——, and Coauthors, 2007: Global climate projections. *Climate Change 2007: The Physical Science Basis,* S. Solomon et al., Eds., Cambridge University Press, 747–845.

——, C. Tebaldi, G. Walton, D. Easterling, and L. McDaniel, 2009: Relative increase of record high maximum temperatures compared to record low minimum temperatures in the U.S. *Geophys. Res. Lett.,* **36,** L23701, doi:10.1029/2009GL040736.

Morak, S., G. C. Hegerl, and J. Kenyon, 2011: Detectable regional changes in the number of warm nights. *Geophys. Res. Lett.,* **38,** L17703, doi:10.1029/2011GL048531.

Quadrelli, R., and J. M. Wallace, 2004: A simplified linear framework for interpreting patterns of Northern Hemisphere wintertime climate variability. *J. Climate,* **17,** 3728–3744.

Rahmstorf, S., and D. Coumou, 2011: Increase of extreme events in a warming world. *Proc. Nat. Acad. Sci.,* **108,** 17 905–17 909, doi:10.1073/pnas.1101766108.

Ruff, T. W., and J. D. Neelin, 2012: Long tails in regional surface temperature probability distributions with implications for extremes under global warming. *Geophys. Res. Lett.,* **39,** L04704, doi:10.1029/2011GL050610.

Schär, C., P. L. Vidale, D. Lüthi, C. Frei, C. Häberli, M. A. Liniger, and C. Appenzeller, 2004: The role of increasing temperature variability in European summer heatwaves. *Nature,* **427,** 332–336.

Seidel, D. J., Q. Fu, W. J. Randel, and T. J. Reichler, 2008: Widening of the tropical belt in a changing climate. *Nat. Geosci.,* **1,** 21–24.

Stott, P. A., D. A. Stone, and M. R. Allen, 2004: Human contribution for the European heatwave of 2003. *Nature,* **432,** 610–614.

Tebaldi, C., K. Hayhoe, J. M. Arblaster, and G. A. Meehl, 2006: Going to the extremes, an intercomparison of model-simulated historical and future changes in extreme events. *Climatic Change,* **79,** 185–211.

Vavrus, S., J. E. Walsh, W. L. Chapman, and D. Portis, 2006: The behavior of extreme cold air outbreaks under greenhouse warming. *Int. J. Climatol.,* **26,** 1133–1147.

Weisheimer, A., F. J. Doblas-Reyes, T. Jung, and T. N. Palmer, 2011: On the predictability of the extreme summer 2003 over Europe. *Geophys. Res. Lett.,* **38,** L05704, doi:10.1029/2010GL046455.

Wettstein, J. J., and L. O. Mearns, 2002: The influence of the North Atlantic–Arctic Oscillation on mean, variance, and extremes of temperature in the Northeastern United States and Canada. *J. Climate,* **15,** 3586–3600.

Yin, J. H., 2005: A consistent poleward shift in the storm tracks in simulations of 21st century climate. *Geophys. Res. Lett.,* **32,** L18701, doi:10.1029/2005GL023684.

Zwiers, F. W., X. Zhang, and Y. Feng, 2011: Anthropogenic influence on long return period daily temperature extremes at regional scales. *J. Climate,* **24,** 881–892.